Forward and Inverse Parameter Estimation Algorithms of Interdigital Dielectrometry Sensors

B. C. Lesieutre, A. V. Mamishev, Y. Du, E. Keskiner, M. Zahn, and G. C. Verghese

Laboratory for Electromagnetic and Electronic Systems
Massachusetts Institute of Technology
Cambridge, MA

ABSTRACT

In this paper we extend the continuum model for interdigital dielectrometry sensors and propose a new, direct technique for estimating material electrical properties from measurements. Interdigital sensors consist of alternating pairs of long, thin electrodes on a plane. An ideal model assumes that the periodic structure extends to infinity and the electrodes have no thickness. We extend this ideal analysis to account for the physical thickness of the electrodes. We also present the model in a matrix form which is amenable to linear algebraic analysis techniques. In particular, the 'inverse problem' of estimating material properties is formulated as a generalized Eigenvalue problem, which avoids the convergence problems of previous iterative algorithms.

1 INTRODUCTION

INTERDIGITAL sensors are used for a wide range of applications including humidity sensors [1], the monitoring of cure processes [2], chemical sensors [3–6], and others. Research is being conducted on their potential use as land-mine detectors [7]. Our research group has been developing interdigital sensors primarily for monitoring moisture dynamics in transformer insulation for the purpose of better understanding the 'flow electrification' failure mechanism [8, 9].

Interdigital electrode sensors serve as useful tools for monitoring the moisture diffusion process for several reasons. When the moisture distribution changes in the material, the electrical conductivity and permittivity will change correspondingly. The sensors are convenient because they only require access to one side of the test material, and, importantly, by combining the measurements from two or more sensors, one can determine the spatial profile of electrical properties. From this information, the spatial profile of moisture can be inferred.

To understand the operation of this type of sensor, consider the generic sensor shown in Figure 1 in which the sensor's copper 'fingers' are shown in black as is the 'ground plane' underneath the sensor. A half-wavelength physical and electrical model is shown in Figure 2.

The material to be tested contacts the sensor on the top (in Figure 1) from only one side of the material under test. A sinusoidal (in time) 'drive' voltage is applied to one set of the electrodes, denoted by V_D in Figure 1, and a 'sensed signal' is measured on the other set of electrodes.

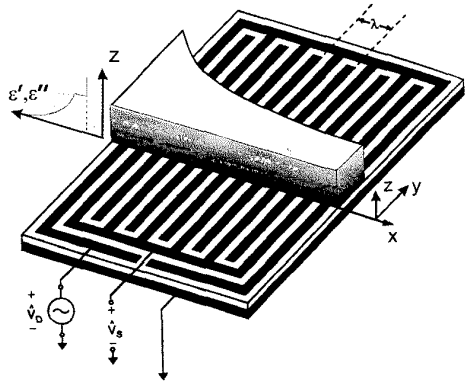

Figure 1. Interdigital Sensor.

Earlier work loaded the sensing electrode with a known capacitor, and the magnitude and phase of the floating voltage V_S of the sensing electrode was measured. Our most recent work has shown better signal to noise characteristics by virtually grounding the sensing electrode at the input of an op-amp and measuring the op-amp output voltage across a known feedback capacitor. The imposed drive and sense voltages create a nearly periodic voltage profile on the sensor surface which is the fundamental characteristic of these sensors.

1070–9878/1/ $3.00

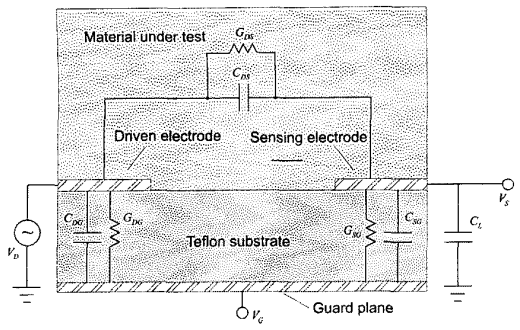

Figure 2. A half-wavelength cross section of an interdigital sensor.

The usefulness of a periodic voltage profile can be seen under idealized physical conditions. Consider an infinite plane sensor spanning the x and y directions on which the surface voltage distribution is a perfect sinusoid in space in the x direction and which is uniform in the y direction. The fundamental spatial frequency of the sinusoid is given by $k_1 = 2\pi/\lambda$ where λ is the spatial period. A homogeneous test material of infinite thickness is placed on top of the sensor. The solution to Laplace's equation in the material requires that the voltage decreases exponentially from the sensor plane/material interface (in the z direction) with an exponential decay rate of $-2\pi/\lambda$. Consequently the electric field also decreases exponentially as $\exp(-2\pi z/\lambda)$ being periodic in the x direction and uniform in the y direction. Since the electric field decays away from the interface, a sensor that measures a terminal current at the sensor surface, which depends on the electric field normal to the surface through conduction and displacement currents, will only 'see' as far as the electric field lines effectively penetrate the material. This 'penetration depth' depends on the spatial wavelength of the sinusoidal voltage in the sensor plane. The electric field will penetrate further for longer wavelength sensors than for shorter wavelength sensors as illustrated in Figure 3.

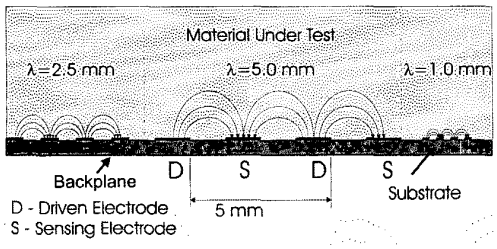

Figure 3. Multiple wavelength penetration depths.

This notion, that a one-sided application of a spatially sinusoidal voltage will give rise to electric fringing fields that penetrate into a material to a certain effective penetration depth which depends on the wavelength, can be exploited to probe into a material at different penetration depths. By analyzing data taken from several sensors with different spatial wavelengths, one can gain information about properties at different depths in the material, allowing the determination of spatial profiles of a material's dielectric properties.

Practical finite-size sensors and measuring environments differ from the ideal in at least four significant ways:

1. the voltage distribution of the sensor cannot extend to infinity in the x direction,
2. the voltage is not completely uniform in the y direction,
3. the test material is not infinitely thick, and
4. a perfect spatial sinusoidal voltage is difficult, if not impossible, to impose on the sensor surface.

Nevertheless, finite size interdigital sensors have the same beneficial features as the ideal. They only require access to one side of the material, and they have fringing fields that penetrate into the test material. Mathematical modeling and physical approximations can be used to account for the non-ideal geometric aspects of the sensors. To minimize end effects due to the truncation of the applied periodic voltage on the electrodes in the x direction, only the sensing electrodes in the center of the structure are used in the measurement. Figure 4 shows a three-wavelength sensor where an isolated lead comes for the sensing electrodes in the middle of the structure for each wavelength. The 'guard fingers' at the ends of the structure are held at the same potential as the middle sensing fingers to make the voltage and electric fields appear in the center region as they would if the structure extended further in the x direction. Laboratory tests have shown that the four end guard fingers shown in Figure 4 reduce end effect errors to <1% [7]. End effects in the y direction are accounted for in the analysis stage using an empirically derived relation and finite-element computer simulations which are presented in [10] and which we use in Section 4 of this paper.

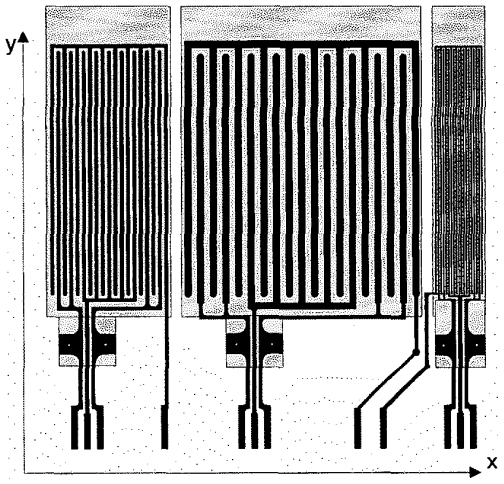

Figure 4. Three-wavelength interdigital sensor.

The last two points, the finite thickness of the test material and the periodic, but not sinusoidal, nature of the voltage requires us to be careful about the solution to Laplace's equation, but do not pose fundamental limitations on the use of the sensor. The periodic voltage can be represented by a Fourier series with harmonics indexed by wavenumber $k_n = 2\pi n/\lambda$. For each spatial harmonic denoted by $n \geq 1$ the voltage will give rise to electric fields that essentially decay at an exponential rate, with exponent equal to the negative of the wavenumber

$\exp(-k_n z)$. The deepest penetration depth occurs for the fundamental spatial wavelength with n=1. The only qualitative difference introduced by the Fourier series representation is for the zeroth-harmonic n=0. The corresponding electric field is then spatially given by the average surface voltage divided by the test material thickness, which is zero for an infinitely thick sample. In most of our laboratory experiments this zero-harmonic component is small and does not provide a reliable means to probe the sample.

In previous work a continuum model was developed to analyze the response of interdigital sensors. We review this model in Section 2. We mention here that one of the simplifying assumptions used in the original development is to treat the electrodes as having no height. That is, they are assumed to exist only in the plane of the sensor surface and will not extend out of it. Our sensors are fabricated using an etching process and consequently the electrodes have heights of order 9 to 35 μm. In our laboratory work it was determined that the effect of the electrode height, creating a 'gap' between the electrodes, is not negligible, especially for smaller wavelength sensors [11]. One of the contributions of the present paper is to extend the continuum model to account for the finite height of the electrodes.

The other main contribution we offer in this paper is an improved method for using the model to estimate material properties from the measured signal. As we shall see in Section 2, the continuum model is well-suited for solving the 'forward problem' of predicting the measurement, given the sensor geometry and knowledge of the electrical properties of all the materials (substrate and test sample). In practice, the purpose of the sensor is to estimate a test material's electrical properties from measurements and knowledge of the sensor's geometry. Previously, this 'inverse problem' was accomplished by repeatedly solving the forward problem, adjusting the estimate at each iteration until the predicted response matched the measurement. This approach did not always work well because it would not always converge or would converge to an answer that was obviously not physical. Additionally, as implemented, the analysis software did not provide error bounds on the estimates due to errors in the measurements. In Section 4 we demonstrate that the continuum model admits many solutions to the inverse problem and we present a method based on 'generalized Eigenanalysis' to find them all. From the complete set of mathematically admissible solutions, one can quickly identify the physically possible solutions and discard the rest. With little extra work, one can also obtain error bounds on the estimate.

2 THE CONTINUUM MODEL

In this Section we review the continuum model. As in the original work [12, 13] we derive the model in the context of solving the 'forward problem'. Given the sensor geometry and known conductivities and permittivities of relevant materials, we compute the expected response of the sensor. Our presentation differs from earlier work in that we consider both a short-circuit and floating voltage measurement mode response, we do not discuss the physics in terms of complex surface capacitances, and we emphasize a matrix formulation which we will exploit when discussing the inverse problem.

Consider Figure 5, where one-half spatial wavelength of a cross section of the sensor is shown in detail. We relate this to the ideal sensor by assuming the electrode structure is infinitely periodic with a spatial period equal to the wavelength, and the electrodes are infinitely long in the y direction which is normal to the x-z cross section shown in the Figure. In practice, we account for the end effects due to the finite length of the electrodes with an empirical correction factor, and the guard electrodes serve to increase the periodicity of the electrode structure in the x direction [7]. Consistent with previous work, in this Section we assume that the electrode height is negligible [12, 13]. In Section 3 we correct for the electrode height.

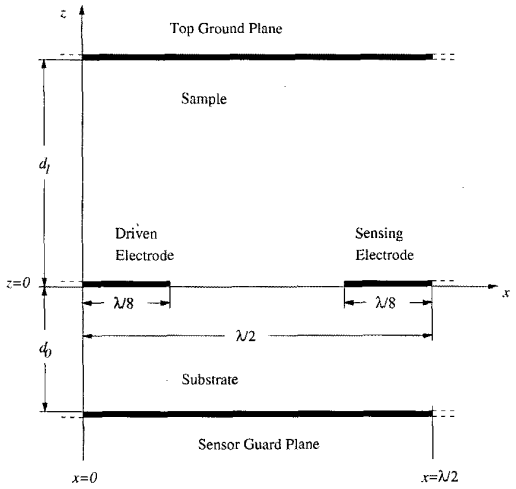

Figure 5. One half wavelength cross section of an interdigital sensor and sample (not drawn to scale).

To calculate the current leaving the sensing electrode we first calculate the electric field normal to the electrode surface. We observe that this calculation is a simple exercise if we know the potential on the sensor/sample interface. Due to the periodic structure of the electrodes, this potential will have a Fourier series representation, and due to the even symmetry due to the choice of the placement of the origin in Figure 5, it has a cosine series representation

$$V(x, z=0) = \sum_{n=0}^{\infty} V_n \cos(k_n x) \tag{1}$$

where

$$k_n = \frac{2\pi n}{\lambda} \tag{2}$$

and λ is the electrode fundamental spatial period.

The voltages in the homogeneous sensor substrate and the homogeneous sample layer satisfy Laplace's equation, $\nabla^2 V$=0, in both regions and is continuous across the interface. It is easily shown that the voltages that satisfy the zero potential boundary conditions at the sensor guard plane at $z = -d_o$ and at the top ground plane at $z = d_1$ and Laplace's equation are given by the following relations

$$V_{su}(x, -d_0 \le z \le 0) = \sum_{n=0}^{\infty} \frac{\sinh(k_n(z+d_0))}{\sinh(k_n d_0)} V_n \cos(k_n x) \tag{3}$$

$$V_{sa}(x, 0 \le z \le d_1) = \sum_{n=0}^{\infty} \frac{-\sinh(k_n(z-d_1))}{\sinh(k_n d_1)} V_n \cos(k_n x) \quad (4)$$

We pause to mention some notation that we will use throughout this paper. The subscripts 'su' and 'sa' indicate values in the substrate and test sample materials respectively. While this distinction is not absolutely necessary for the scalar potential in (3) and (4), it will provide clarity for other quantities in subsequent equations. From (3) and (4), the z component of the electric field normal to the sensing electrode can be readily evaluated. In the substrate

$$E_{z,su}(x, z=0) = -\left.\frac{\partial V_{su}}{\partial z}\right|_{z=0} = \sum_{n=0}^{\infty} \frac{-\cosh(k_n d_0)}{\sinh(k_n d_0)} k_n V_n \cos(k_n x) \quad (5)$$

and in the sample,

$$E_{z,sa}(x, z=0) = -\left.\frac{\partial V_{sa}}{\partial z}\right|_{z=0} = \sum_{n=0}^{\infty} \frac{\cosh(k_n(d_1))}{\sinh(k_n d_1)} k_n V_n \cos(k_n x) \quad (6)$$

The complex amplitude of the total current density at radian frequency ω due to the conduction and displacement current densities onto the electrode surface is given by

$$J = (\sigma_{su} + i\omega\varepsilon_{su}) E_{z,su}(x, z=0) - (\sigma_{sa} + i\omega\varepsilon_{sa}) E_{z,sa}(x, z=0) \quad (7)$$

and is uniform along the length of the electrode (y direction). A one-dimensional current per unit length in the y direction for half of each sensing electrode can be calculated by integrating (7) along the half width of the electrode (x direction) and is given by

$$J_s = \int_{\frac{3\lambda}{8}}^{\frac{\lambda}{2}} J\,dx = (\sigma_{su} + i\omega\varepsilon_{su}) \sum_{n=0}^{\infty} \frac{-\cosh(k_n d_0)}{\sinh(k_n d_0)} V_n \times \left(\sin\left(\frac{\lambda k_n}{2}\right) - \sin\left(\frac{3\lambda k_n}{8}\right)\right) - (\sigma_{sa} + i\omega\varepsilon_{sa}) \sum_{n=0}^{\infty} \frac{\cosh(k_n d_1)}{\sinh(k_n d_1)} V_n \times \left(\sin\left(\frac{\lambda k_n}{2}\right) - \sin\left(\frac{3\lambda k_n}{8}\right)\right) \quad (8)$$

The total sensing electrode current measured from the sensor is then obtained by

$$I_s = J_s L_{eff} \quad (9)$$

where L_{eff} is twice the effective length of the sensing electrode structure since (8) only calculates the current over one half of the sensing electrode.

As we mentioned earlier, obtaining result (8) is an elementary exercise once the voltage on the sensor/sample interface is known so that V_n are known for all n. Note that not all periodic voltage profiles are allowed on this interface, and the method of measurement, sensing electrode short-circuit mode or floating voltage mode, will affect the voltage profile. The electric field across the interface must satisfy the continuity equation (neglecting surface effects here)

$$(\sigma_{su} + i\omega\varepsilon_{su}) E_{z,su} = (\sigma_{sa} + i\omega\varepsilon_{sa}) E_{z,sa} \quad \text{for} \quad \frac{\lambda}{8} \le x \le \frac{3\lambda}{8}, \quad z = 0 \quad (10)$$

Using a capacitively loaded floating voltage measurement, the measured sensing electrode current and voltage are constrained by

$$I_s = i\omega C_L V_S \quad (11)$$

where C_L is the value of the capacitance for the known load capacitor. In short circuit measurement mode the sensing electrode voltage is simply

$$V_S = 0 \quad (12)$$

The challenge is to find a voltage profile on the interface that simultaneously satisfies the applied driven electrode potential, the continuity, Equation (10), and the relevant terminal constraint given by (11) or (12). In this paper, as in previous work [12–14], this is accomplished by approximating the voltage profile by a piecewise continuous function as shown in Figure 6. Under this approximation the problem reduces to determining the values of the voltages at the 'collocation points', x_1, x_2, and x_3 in Figure 6, where $\lambda/8 < x_i < 3\lambda/8$. More generally we choose p collocation points where p depends on the desired accuracy of the representation. The collocation points may be distributed uniformly on the surface, however, typically the points should be placed more densely near the electrodes where the voltage is expected to undergo larger changes. Mathematically, to determine unknown voltages at p collocation points, we require p independent constraint equations to solve. To this end we require the continuity equation to be satisfied over an interval surrounding each collocation point. Specifically we require for each $1 \le i \le p$

$$\int_{\frac{x_{i-1}+x_i}{2}}^{\frac{x_{i+1}+x_i}{2}} \left((\sigma_{su} + i\omega\varepsilon_{su}) E_{z,su}(x, z=0) - (\sigma_{sa} + i\omega\varepsilon_{sa}) E_{z,sa}(x, z=0)\right) dx = 0 \quad (13)$$

where $x_0 = \lambda/4 - x_1$ and $x_{p+1} = 3\lambda/4 - x_p$ to make the endpoints occur at the electrode edges.

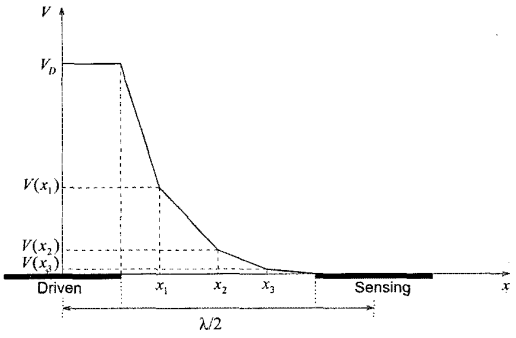

Figure 6. Collocation point voltages (adapted from [14]).

Note that $E_{z,\mathrm{su}}(x, z = 0)$ and $E_{z,\mathrm{sa}}(x, z = 0)$ are expressed in terms of the Fourier series representation for the voltage in (5) and (6). The relationship between the Fourier series coefficients and the collocation point voltages is easily obtained [13]. Assuming a truncated Fourier series with $m + 1$ terms, the relationship between the collocation point voltages can be expressed in matrix form by

$$\begin{bmatrix} V_0 \\ \vdots \\ V_m \end{bmatrix} = \mathbf{T} \begin{bmatrix} V_D \\ V(x_1) \\ \vdots \\ V(x_p) \\ V_S \end{bmatrix} \tag{14}$$

where V_D and V_S represent the driven and sensing electrode voltages respectively. Matrix $\mathbf{T} \in \mathcal{R}((m+1)\times(p+2))$ (a real-valued $m+1$ by $p+2$ matrix) and the values of the elements are listed in the Appendix.

In terms of harmonic coefficients, constraint (13) can also be written in matrix form as

$$[(\sigma_{\mathrm{su}} + \mathrm{i}\omega\varepsilon_{\mathrm{su}})\mathbf{A} - (\sigma_{\mathrm{sa}} + \mathrm{i}\omega\varepsilon_{\mathrm{sa}})\mathbf{B}] \begin{bmatrix} V_0 \\ \vdots \\ V_m \end{bmatrix} = \begin{bmatrix} 0 \\ \vdots \\ 0 \end{bmatrix} \tag{15}$$

where the elements of $\mathbf{A} \in \mathcal{R}(p\times(m+1))$ and $\mathbf{B} \in \mathcal{R}(p\times(m+1))$ are

$$a_{i,k} = \frac{-\cosh(k_n d_0)}{\sinh(k_n d_0)} \left[\sin\left(k_n \left(\frac{x_{i+1}+x_i}{2}\right)\right) - \sin\left(k_n \left(\frac{x_{i-1}+x_i}{2}\right)\right)\right] \tag{16}$$

and

$$b_{i,k} = \frac{\cosh(k_n d_1)}{\sinh(k_n d_1)} \left[\sin\left(k_n \left(\frac{x_{i+1}+x_i}{2}\right)\right) - \sin\left(k_n \left(\frac{x_{i-1}+x_i}{2}\right)\right)\right] \tag{17}$$

Combining (14) and (15) gives

$$[(\sigma_{\mathrm{su}} + \mathrm{i}\omega\varepsilon_{\mathrm{su}})\mathbf{AT} - (\sigma_{\mathrm{sa}} + \mathrm{i}\omega\varepsilon_{\mathrm{sa}})\mathbf{BT}] \begin{bmatrix} V_D \\ V(x_1) \\ \vdots \\ V(x_p) \\ V_S \end{bmatrix} = \begin{bmatrix} 0 \\ \vdots \\ 0 \end{bmatrix} \tag{18}$$

which represents p equations in terms of $p + 1$ unknowns since V_D is known.

The relation for J_s is already given by (8); in matrix form this is

$$J_s = [(\sigma_{\mathrm{su}} + \mathrm{i}\omega\varepsilon_{\mathrm{su}})\mathbf{CT} - (\sigma_{\mathrm{sa}} + \mathrm{i}\omega\varepsilon_{\mathrm{sa}})\mathbf{DT}] \begin{bmatrix} V_D \\ V(x_1) \\ \vdots \\ V(x_p) \\ V_S \end{bmatrix} \tag{19}$$

where

$$c_{i,n} = \frac{-\cosh(k_n d_0)}{\sinh(k_n d_0)} \left[\sin\left(k_n \frac{\lambda}{2}\right) - \sin\left(k_n \frac{3\lambda}{8}\right)\right] \tag{20}$$

and

$$d_{i,n} = \frac{\cosh(k_n d_1)}{\sinh(k_n d_1)} \left[\sin\left(k_n \frac{\lambda}{2}\right) - \sin\left(k_n \frac{3\lambda}{8}\right)\right] \tag{21}$$

Along with the sensing electrode terminal constraint given by either (11) or (12), Equations (18) and (19) can be solved for the values of $V(x_1) \cdots V(x_p)$ and J_s, using straightforward linear algebra.

We pause to mention that this presentation emphasizes the explicit dependence on $(\sigma_{\mathrm{sa}} + \mathrm{i}\omega\varepsilon_{\mathrm{sa}})$ which we will exploit in Section 4 to solve the 'inverse problem'. In summary, the solution to (18) represents a piecewise continuous sensor/sample interface voltage profile which satisfies the continuity Equations (13), and (19) gives the solution for the sensing electrode current density.

In practice, the purpose of the sensor is to determine the electrical properties $(\sigma_{\mathrm{sa}} + \mathrm{i}\omega\varepsilon_{\mathrm{sa}})$ from a knowledge of the sensor/sample geometry and a measurement of the sensing electrode short-circuit current. This is typically accomplished by repeatedly solving the 'forward problem' defined by Equations (18) and (19) and the terminal constraint (11) or (12). The value of $(\sigma_{\mathrm{sa}} + \mathrm{i}\omega\varepsilon_{\mathrm{sa}})$ at each iteration is adjusted to reduce the difference between the predicted and measured responses.

This approach has several shortcomings. Firstly, from extensive experimentation it has been determined that the physical height of the electrodes cannot be neglected. The gap between the electrodes can introduce a noticeable error in the calculations and needs to be included in the model. Secondly, the iterative procedure outlined above will not always converge, or will sometimes converge to an incorrect and physically impossible answer.

In this paper we augment the model to take into account the height of the electrodes and present an efficient method to find all possible mathematical solutions to the "inverse problem" for the single unknown layer case from which all physically reasonable solutions can be extracted.

3 ELECTRODE HEIGHT

In this Section we augment our model to account for the height of the electrodes. We again follow the ideas of the continuum model by approximating the voltage on the sensor/sample interface by a piecewise continuous function determined by the voltages at certain collocation points. However, now we define two surfaces: one level with the bottom of the electrodes at $z = 0$ and another level with the top of the electrodes at $z = h$ (Figure 7).

In each of the three homogeneous regions, the 'substrate', 'gap', and 'sample', the voltages satisfy Laplace's equation. The voltages on the surfaces $z = 0$ and $z = h$ can be represented by a Fourier cosine series

$$V_{\mathrm{su}}(x, z = 0) = \sum_{n=0}^{\infty} V_{0,n} \cos(k_n x) \tag{22}$$

$$V_{\mathrm{sa}}(x, z = h) = \sum_{n=0}^{\infty} V_{h,n} \cos(k_n x) \tag{23}$$

The notational subscripts '0' and 'h' are used to refer to the levels $(z = 0)$ and $(z = h)$ respectively. In this Section we also introduce the subscript 'gap' to denote quantities in the region between the electrodes.

It can be shown easily that the potential in the substrate region is given by

$$V_{\mathrm{su}}(x, -d_0 \le z \le 0) = \sum_{n=0}^{\infty} \frac{\sinh[k_n(z + d_0)]}{\sinh(k_n d_0)} V_{0,n} \cos(k_n x) \tag{24}$$

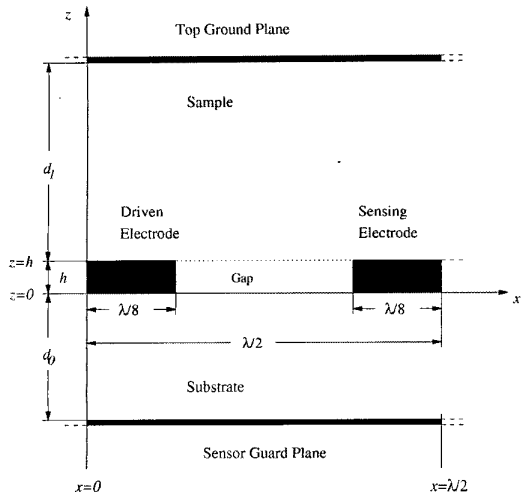

Figure 7. One half wavelength cross section of an interdigital sensor and sample. This is not shown to scale, rather, it is drawn to emphasize the relevant structure including the height of the electrodes.

Likewise, the voltage in the sample region can be expressed as

$$V_{\text{sa}}(x, h \le z \le h + d_1) = \sum_{n=0}^{\infty} \frac{-\sinh\left[k_n(z-h-d_1)\right]}{\sinh(k_n d_1)} V_{h,n} \cos(k_n x) \quad (25)$$

In the 'gap' region between the electrodes it is convenient to employ a different representation for the voltages at the gap/sample interface at $z = h$ and the gap/substrate interface at z=0. These are given by

$$V_{\text{g}}(\tfrac{\lambda}{8} \le x \le \tfrac{3\lambda}{8}, z = h) = V_D - \frac{(V_D - V_S)(x - \frac{\lambda}{8})}{\frac{\lambda}{4}} + \sum_{n=1}^{\infty} V_{\text{g},h,n} \sin\left(2k_n\left(x - \tfrac{\lambda}{8}\right)\right) \quad (26)$$

$$V_{\text{g}}(\tfrac{\lambda}{8} \le x \le \tfrac{3\lambda}{8}, z = 0) = V_D - \frac{(V_D - V_S)(x - \frac{\lambda}{8})}{\frac{\lambda}{4}} + \sum_{n=1}^{\infty} V_{\text{g},0,n} \sin\left(2k_n\left(x - \tfrac{\lambda}{8}\right)\right) \quad (27)$$

The terms linear in x in (26) and (27) represent a particular solution to Laplace's equation that satisfies the boundary conditions at the electrode surfaces at $x = \lambda/8$ ($V = V_D$) and $x = 3\lambda/8$ ($V = V_S$). To this we add a sine series representation to match the boundary conditions at $z = 0$ and $z = h$ in the gap region. Since the contribution of the sine series to the voltage must be zero at $x = \lambda/8$ and $x = 3\lambda/8$, the lowest fundamental frequency for the series is $2k_n$ which corresponds to a half-wavelength (in the sine series) equal to the size of the $\lambda/4$ gap between the electrodes. Thus, $\sin(2k_n(x - \lambda/8)) = 0$ at $x = \lambda/8$ and $x = 3\lambda/8$ for all n.

The solution to Laplace's equation in the gap region is given by

$$V_{\text{g}}(\tfrac{\lambda}{8} \le x \le \tfrac{3\lambda}{8}, 0 \le z \le h) = V_D - \frac{(V_D - V_S)(x - \frac{\lambda}{8})}{\lambda/4} + \sum_{n=1}^{\infty} \frac{\sinh(2k_n z)}{\sinh(2k_n h)} V_{\text{g},h,n} \sin\left[2k_n\left(x - \tfrac{\lambda}{8}\right)\right] - \sum_{n=1}^{\infty} \frac{\sinh(2k_n(z-h))}{\sinh(2k_n h)} V_{\text{g},0,n} \sin\left[2k_n\left(x - \tfrac{\lambda}{8}\right)\right] \quad (28)$$

As in Section 2, we approximate the voltage profile at these two surfaces by piecewise continuous functions described by the potentials at certain collocation points. We choose p collocation points on each surface denoted by $x_{0,1} \cdots x_{0,p}$ and $x_{h,1} \cdots x_{h,p}$. Assuming a truncated Fourier series representation of $(m_1 + 1)$ harmonics for (22) and (23) and (m_2+1) harmonics for (26) and (27), one can relate the collocation point voltages and Fourier series coefficients through

$$\begin{bmatrix} V_{\text{sa},h,0} \\ \vdots \\ V_{\text{sa},h,m_1} \end{bmatrix} = \mathbf{T_1} \begin{bmatrix} V_D \\ V(x_{h,1}) \\ \vdots \\ V(x_{h,p}) \\ V_S \end{bmatrix} \quad (29)$$

$$\begin{bmatrix} V_{\text{su},0,0} \\ \vdots \\ V_{\text{su},0,m_1} \end{bmatrix} = \mathbf{T_1} \begin{bmatrix} V_D \\ V(x_{0,1}) \\ \vdots \\ V(x_{0,p}) \\ V_S \end{bmatrix} \quad (30)$$

$$\begin{bmatrix} V_{\text{g},h,0} \\ \vdots \\ V_{\text{g},h,m_2} \end{bmatrix} = \mathbf{T_2} \begin{bmatrix} V_D \\ V(x_{h,1}) \\ \vdots \\ V(x_{h,p}) \\ V_S \end{bmatrix} \quad (31)$$

$$\begin{bmatrix} V_{\text{g},0,0} \\ \vdots \\ V_{\text{g},0,m_2} \end{bmatrix} = \mathbf{T_2} \begin{bmatrix} V_D \\ V(x_{0,1}) \\ \vdots \\ V(x_{0,p}) \\ V_S \end{bmatrix} \quad (32)$$

where Matrix $\mathbf{T_1}$ is identical to $\mathbf{T}$ in (14) and $\mathbf{T_1}$ and $\mathbf{T_2}$ are given in the appendix.

There are $2p$ unknown collocation point voltages and we form $2p$ continuity constraint equations, p at each surface; for $1 \le i \le p$

$$0 = \int_{\frac{x_{0,i-1}+x_{0,i}}{2}}^{\frac{x_{0,i+1}+x_{0,i}}{2}} \left((\sigma_{\text{su}} + \text{i}\omega\varepsilon_{\text{su}})E_{z,\text{su}}(x, z=0) - (\sigma_{\text{g}} + \text{i}\omega\varepsilon_{\text{g}})E_{z,\text{g}}(x, z=0)\right) dx \quad (33)$$

$$0 = \int_{\frac{x_{h,i-1}+x_{h,i}}{2}}^{\frac{x_{h,i+1}+x_{h,i}}{2}} \left((\sigma_{\text{sa}} + \text{i}\omega\varepsilon_{\text{sa}})E_{z,\text{sa}}(x, z=h) - (\sigma_{\text{g}} + \text{i}\omega\varepsilon_{\text{g}})E_{z,\text{g}}(x, z=h)\right) dx \quad (34)$$

In terms of the Fourier series coefficients,

$$E_{z,\text{su}}(x, z=0) = \sum_{n=0}^{m_1} \frac{-\cosh(k_n d_0)}{\sinh(k_n d_0)} k_n V_{0,n} \cos(k_n x) \quad (35)$$

$$E_{z,\mathrm{sa}}(x, z=h) = \sum_{n=0}^{m_1} \frac{\cosh(k_n d_1)}{\sinh(k_n d_1)} k_n V_{h,n} \cos(k_n x) \quad (36)$$

$$E_{z,\mathrm{g}}(\tfrac{\lambda}{8} \le x \le \tfrac{3\lambda}{8}, z=0) = \sum_{n=1}^{m_2} \frac{-1}{\sinh(2k_n h)} 2k_n V_{\mathrm{g},h,n} \sin(2k_n(x-\tfrac{\lambda}{8})) + \sum_{n=1}^{m_2} \frac{\cosh(2k_n h)}{\sinh(2k_n h)} 2k_n V_{\mathrm{g},0,n} \sin(2k_n(x-\tfrac{\lambda}{8})) \quad (37)$$

$$E_{z,\mathrm{g}}(\tfrac{\lambda}{8} \le x \le \tfrac{3\lambda}{8}, z=h) = \sum_{n=1}^{m_2} \frac{-\cosh(2k_n h)}{\sinh(2k_n h)} 2k_n V_{\mathrm{g},h,n} \sin(2k_n(x-\tfrac{\lambda}{8})) + \sum_{n=1}^{m_2} \frac{1}{\sinh(2k_n h)} 2k_n V_{\mathrm{g},0,n} \sin(2k_n(x-\tfrac{\lambda}{8})) \quad (38)$$

Using (35) to (38), the constraint equations in matrix form can be written as

$$(\sigma_{\mathrm{su}} + \mathrm{i}\omega\varepsilon_{\mathrm{su}})\mathbf{A}_{\mathrm{su}} \begin{bmatrix} V_{0,0} \\ \vdots \\ V_{0,m_1} \end{bmatrix} - (\sigma_{\mathrm{g}} + \mathrm{i}\omega\varepsilon_{\mathrm{g}})\times \left[\mathbf{A_{g1}} \begin{bmatrix} V_{\mathrm{g},0,0} \\ \vdots \\ V_{\mathrm{g},0,m_2} \end{bmatrix} + \mathbf{A_{g2}} \begin{bmatrix} V_{\mathrm{g},h,0} \\ \vdots \\ V_{\mathrm{g},h,m_2} \end{bmatrix} \right] = 0 \quad (39)$$

and

$$(\sigma_{\mathrm{sa}} + \mathrm{i}\omega\varepsilon_{\mathrm{sa}})\mathbf{A}_{\mathrm{sa}} \begin{bmatrix} V_{0,0} \\ \vdots \\ V_{0,m_1} \end{bmatrix} - (\sigma_{\mathrm{g}} + \mathrm{i}\omega\varepsilon_{\mathrm{g}})\times \left[-\mathbf{A_{g2}} \begin{bmatrix} V_{\mathrm{g},0,0} \\ \vdots \\ V_{\mathrm{g},0,m_2} \end{bmatrix} - \mathbf{A_{g1}} \begin{bmatrix} V_{\mathrm{g},h,0} \\ \vdots \\ V_{\mathrm{g},h,m_2} \end{bmatrix} \right] = 0 \quad (40)$$

where

$$A_{\mathrm{su},i,n} = \frac{-\cosh(k_n d_0)}{\sinh(k_n d_0)}\times \left[\sin\left(k_n\left(\frac{x_{0,i+1}+x_{0,i}}{2}\right)\right) - \sin\left(k_n\left(\frac{x_{0,i-1}+x_{0,i}}{2}\right)\right)\right] \quad (41)$$

$$A_{\mathrm{sa},i,n} = \frac{\cosh(k_n d_1)}{\sinh(k_n d_1)}\times \left[\sin\left(k_n\left(\frac{x_{h,i+1}+x_{h,i}}{2}\right)\right) - \sin\left(k_n\left(\frac{x_{h,i-1}+x_{h,i}}{2}\right)\right)\right] \quad (42)$$

$$A_{\mathrm{g2},i,n} = \frac{1}{\sinh(2k_n h)}\times \left[\cos\left(2k_n\left(\frac{x_{0,i+1}+x_{0,i}}{2}\right)\right) - \cos\left(2k_n\left(\frac{x_{0,i-1}+x_{0,i}}{2}\right)\right)\right] \quad (43)$$

$$A_{\mathrm{g1},i,n} = \frac{-\cosh(2k_n h)}{\sinh(2k_n h)}\times \left[\cos\left(2k_n\left(\frac{x_{h,i+1}+x_{h,i}}{2}\right)\right) - \cos\left(2k_n\left(\frac{x_{h,i-1}+x_{h,i}}{2}\right)\right)\right] \quad (44)$$

Combining with (29) to (32) gives

$$(\sigma_{\mathrm{su}} + \mathrm{i}\omega\varepsilon_{\mathrm{su}}) \begin{bmatrix} \mathbf{A_{su}T_1} & 0 \\ 0 & 0 \end{bmatrix} - (\sigma_{\mathrm{g}} + \mathrm{i}\omega\varepsilon_{\mathrm{g}}) \begin{bmatrix} \mathbf{A_{g1}T_2} & \mathbf{A_{g2}T_2} \\ -\mathbf{A_{g2}T_2} & -\mathbf{A_{g1}T_2} \end{bmatrix} + (\sigma_{\mathrm{sa}} + \mathrm{i}\omega\varepsilon_{\mathrm{sa}}) \begin{bmatrix} 0 & 0 \\ 0 & \mathbf{A_{sa}T_1} \end{bmatrix} \begin{bmatrix} \mathbf{v_0} \\ \mathbf{v_h} \end{bmatrix} = \begin{bmatrix} \mathbf{0} \\ \mathbf{0} \end{bmatrix} \quad (45)$$

where

$$\mathbf{v_0} = [V_D\ V(x_{0,1}) \cdots V(x_{0,n})\ V_S]^T \quad (46)$$

$$\mathbf{v_h} = [V_D\ V(x_{h,1}) \cdots V(x_{h,n})\ V_S]^T \quad (47)$$

Equation (45) represents $2n$ equations in terms of $2n$ unknown collocation point voltages since V_D is known and V_S is constrained by either (11) or (12).

The one-dimensional current density leaving the sensing electrode is also easily calculated as before. Note that we need to take into account the contribution on the side of the electrodes at $x = 3\lambda/8$. The electric field here is given by

$$E_{x,\mathrm{g}}(x=\frac{3\lambda}{8}, 0 \le z \le h) = -\left.\frac{\partial V_{\mathrm{g}}}{\partial x}\right|_{x=3\lambda/8} = \frac{(V_D - V_S)}{\lambda/4} - \sum_{n=1}^{m_2} \frac{\sinh(2k_n z)}{\sinh(2k_n h)} 2k_n V_{\mathrm{g},h,n} \cos(2k_n \tfrac{\lambda}{4}) + \sum_{n=1}^{m_2} \frac{\sinh(2k_n(z-h))}{\sinh(2k_n h)} 2k_n V_{\mathrm{g},0,n} \cos(2k_n \tfrac{\lambda}{4}) \quad (48)$$

The one-dimensional current density is obtained from the integration of (8) plus an integration over the gap height

$$\int_0^h (\sigma_{\mathrm{g}} + \mathrm{i}\omega\varepsilon_{\mathrm{g}}) E_{x,\mathrm{g}} dz \quad (49)$$

to yield

$$J_s = -(\sigma_{\mathrm{su}} + \mathrm{i}\omega\varepsilon_{\mathrm{su}})\times \sum_{n=0}^{m_1} \frac{\cosh(k_n d_0)}{\sinh(k_n d_0)} V_{0,n} \left[-\sin(k_n \tfrac{3\lambda}{8})\right] - (\sigma_{\mathrm{sa}} + \mathrm{i}\omega\varepsilon_{\mathrm{sa}})\times \sum_{n=0}^{m_1} \frac{\cosh(k_n d_1)}{\sinh(k_n d_1)} V_{h,n} \left[-\sin(k_n \tfrac{3\lambda}{8})\right] + (\sigma_{\mathrm{g}} + \mathrm{i}\omega\varepsilon_{\mathrm{g}}) \left[\frac{(V_D - V_S)}{\frac{\lambda}{4}} h - \sum_{n=1}^{m_2} \left(\frac{\cosh(2k_n h) - 1}{\sinh(2k_n h)}\right) \times (V_{\mathrm{g},0,n} + V_{\mathrm{g},h,n}) \cos(2k_n \tfrac{\lambda}{4})\right] \quad (50)$$

Equation (50) can be conveniently written in matrix form in terms of collocation point voltages

$$J_s = \left[(\sigma_{su} + i\omega\varepsilon_{su})\,[\mathbf{B}_{su}\mathbf{T_1}\ \ \mathbf{0}]\right. \\ + (\sigma_g + i\omega\varepsilon_g)\,[\mathbf{B_{g0}} + \mathbf{B_{g1}T_2}\ \ -\mathbf{B_{g1}T_2}] \\ \left. + (\sigma_{sa} + i\omega\varepsilon_{sa})\,[\mathbf{0}\ \ -\mathbf{B}_{sa}\mathbf{T_1}]\right]\begin{bmatrix}\mathbf{v_0}\\ \mathbf{v_h}\end{bmatrix} \quad (51)$$

where

$$B_{su,i,n} = \frac{\cosh(k_n d_0)}{\sinh(k_n d_0)}\left(\sin(k_n \tfrac{3\lambda}{8})\right) \quad (52)$$

$$B_{sa,i,n} = \frac{\cosh(k_n d_1)}{\sinh(k_n d_1)}\left(\sin(k_n \tfrac{3\lambda}{8})\right) \quad (53)$$

$$B_{g0,i,n} = \left[\tfrac{h}{\lambda/4}\ \ 0\ \cdots\ 0\ \ \tfrac{-h}{\lambda/4}\right] \quad (54)$$

$$B_{g1,i,n} = -\frac{(\cosh(2k_n h) - 1)}{\sinh(2k_n h)}\cos(2k_n \tfrac{\lambda}{4}) \quad (55)$$

Equations (45) and (51) along with the sensing electrode terminal constraint, (11) or (12), constitute an extended continuum model that accounts for the height of the sensor electrodes. As expressed here in matrix form, they are easily solved using straightforward linear algebra. In the next section we explore how the matrix form of this model can be exploited to efficiently solve the inverse problem.

4 THE INVERSE PROBLEM FOR SHORT-CIRCUIT MODE

Interdigital sensors are intended to be used to measure a sample material's electrical properties. Thus, the unknown in the model is $(\sigma_{sa} + i\omega\varepsilon_{sa})$, and J_s is measured or calculated from measurements assuming we are conducting a short-circuit mode measurement (V_S=0). To study the possible solutions to this problem we combine (45) and (51) into the following form

$$[\mathbf{A} - (\sigma_{sa} + i\omega\varepsilon_{sa})\mathbf{B}]\mathbf{v} = \begin{bmatrix}0\\ \vdots\\ 0\\ J_s\end{bmatrix} \quad (56)$$

where

$$\mathbf{v} = [V_D\ \ V(x_{0,1})\ \cdots\ V(x_{0,n})\ \ V(x_{h,1})\ \cdots\ V(x_{h,n})]^T \quad (57)$$

Matrix $\mathbf{A}$ combines all known quantities in (45) and (51) and $\mathbf{B}$ combines all the known matrices scaled by the unknown $(\sigma_{sa} + i\omega\varepsilon_{sa})$. Note that some minor linear algebra is required to obtain (56) since V_D appears twice in (45) and (51), in both $\mathbf{v_0}$ and $\mathbf{v_h}$, and $V_S = 0$.

To see how (56) can be solved for $(\sigma_{sa} + i\omega\varepsilon_{sa})$ we move the J_s term from the right side of the equation into Matrix $\mathbf{A}$

$$\left[\mathbf{A} - \begin{bmatrix}0 & 0 & \cdots & 0\\ \vdots & & & \vdots\\ 0 & 0 & \cdots & 0\\ \frac{J_s}{V_D} & 0 & \cdots & 0\end{bmatrix} - (\sigma_{sa} + i\omega\varepsilon_{sa})\mathbf{B}\right]\mathbf{v} = \begin{bmatrix}0\\ \vdots\\ 0\\ 0\end{bmatrix} \quad (58)$$

or more compactly written

$$\left[\mathbf{A}' - (\sigma_{sa} + i\omega\varepsilon_{sa})\mathbf{B}\right]\mathbf{v} = \begin{bmatrix}0\\ \vdots\\ 0\\ 0\end{bmatrix} \quad (59)$$

Equation (59) is in the form of a 'generalized Eigenvalue problem' [15] commonly written in the form

$$[\mathbf{M} - \lambda\mathbf{E}]\,\mathbf{v} = \mathbf{0} \quad (60)$$

where λ is called a 'generalized Eigenvalue' and $\mathbf{v}$ is called a 'generalized right Eigenvector'. Techniques for efficiently solving for λ and $\mathbf{v}$ are known and included in common software packages.

Thus, once we have our model in the form given by (59), we can solve for the possible values for the unknown sample's electrical properties – they are the generalized Eigenvalues of (59). The corresponding Eigenvectors are generically unique subject to a scaling. Choosing a scaling such that the first entry is V_D, the other elements of the Eigenvector give the values of the collocation point voltages. We note that depending on the ranks of $\mathbf{A}'$ and $\mathbf{B}$, (59) admits many generalized Eigenvalues. Therefore the solution to the inverse problem, as described by the continuum model, is not unique. For the type of problem considered in this paper, a single homogeneous layer sample, there tends to be a single reasonable solution and many non-physical solutions introduced by the discretization.

This Eigenvalue approach allows us to evaluate how errors in the measurement of J_s affect the estimate of $(\sigma_{sa} + i\omega\varepsilon_{sa})$. Let $\mathbf{v}$ be the generalized right Eigenvector associated with the generalized Eigenproblem

$$\left[\mathbf{A}' - (\sigma_{sa} + i\omega\varepsilon_{sa})\mathbf{B}\right]\mathbf{v} = \mathbf{0} \quad (61)$$

and let $\mathbf{w}$ be the generalized left Eigenvector associated with the generalized Eigenproblem defined by

$$\mathbf{w}^{\mathbf{T}}\left[\mathbf{A}' - (\sigma_{sa} + i\omega\varepsilon_{sa})\mathbf{B}\right] = \mathbf{0} \quad (62)$$

The sensitivity of $(\sigma_{sa} + i\omega\varepsilon_{sa})$ to small variations in Matrix $\mathbf{A}'$ is given by

$$(\Delta\sigma_{sa} + i\omega\Delta\varepsilon_{sa}) = \frac{\mathbf{w^T}\Delta\mathbf{A}'\mathbf{v}}{\mathbf{w^T B v}} \quad (63)$$

Note that the measurement only appears in a single entry of $\mathbf{A}'$, and that (63) can be written as

$$(\Delta\sigma_{sa} + i\omega\Delta\varepsilon_{sa}) = \frac{\mathbf{w^T}\begin{bmatrix}0 & 0 & \cdots & 0\\ \vdots & & & \vdots\\ 0 & 0 & \cdots & 0\\ -1 & 0 & \cdots & 0\end{bmatrix}\mathbf{v}}{\mathbf{w^T B v}}\left(\frac{\Delta J_s}{V_D}\right) \\ = -\frac{w_n v_1}{\mathbf{w^T B v}}\left(\frac{\Delta J_s}{V_D}\right) \quad (64)$$

At this point it is necessary to discuss how the current is measured to relate uncertainties in the actual measurements to the estimates. The short circuit current density is not measured directly, rather a voltage proportional to the short circuit current is measured. The short circuit current is related to its density by

$$I_s = J_s\,(M_L + 1.2\lambda) \quad (65)$$

where M_L is the nominal 'meander length' of the sensing electrodes and the 1.2λ term is an empirically determined correction factor to account for the end effects of the electrodes [10]. The short circuit current is measured by the circuitry shown in Figure 8. The measured voltage is related to the current and the current density by

$$V_L = \frac{-I_s}{i\omega C_F} = \frac{-J_s\,(M_L + 1.2\lambda)}{i\omega C_F} \quad (66)$$

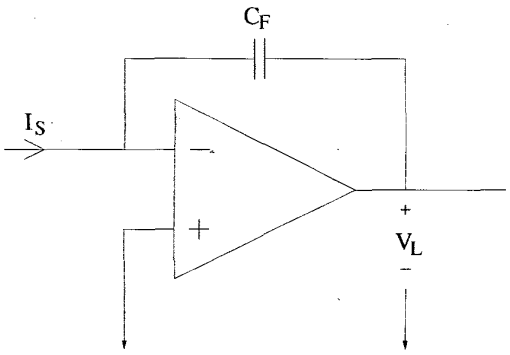

Figure 8. Sensing circuitry.

The sensitivity of the computed short-circuit density J_s to variations in the voltage phasor V_L is expressed by

$$\Delta J_s = \frac{-\mathrm{i}\omega C_F}{(M_L + 1.2\lambda)} \Delta V_L \tag{67}$$

We find it convenient to consider the voltage phasor in polar coordinates with the magnitude given in decibels and the phase in degrees. Likewise, our knowledge of uncertainty in our measurements is in terms of the voltage magnitude in decibels and phase in degrees. Denote the voltage magnitude in decibels by V_{dB} and the phase by ϕ_V. Then the measured voltage phasor in rectangular coordinates is given by

$$V_L = 10^{\frac{V_{dB}}{20}} \exp\left[\mathrm{i}\tfrac{\pi}{180}\phi_V\right] \tag{68}$$

The sensitivity of the measured voltage to uncertainty in the measured voltage magnitude in decibels is

$$\Delta V_L = V_L \frac{\ln(10)}{20} \Delta V_{dB} \tag{69}$$

and the sensitivity to the phase is

$$\Delta V_L = V_L \frac{\pi \mathrm{i}}{180} \Delta\phi_V \tag{70}$$

Equations (64) and (67), along with (69) and (70), can be used to calculate uncertainties in the estimates due to uncertainties in the measurements of voltage magnitude and phase. A 'worst case' estimate of uncertainty combines the effects of both the magnitude and phase uncertainties.

5 DEMONSTRATIONS

In this Section we demonstrate some of the observations and claims of previous Sections. Using the extended continuum model of Section 3 we calculate the response of an interdigital sensor in air for a range of electrode thicknesses. For a demonstration of the inverse problem we calculate all the generalized Eigenvalues, each representing a possible solution, and show that for the case of a single homogeneous layer, only a single solution is physically meaningful and the rest are artifacts of the discretization. For the physically meaningful solution, we also include an uncertainty analysis.

We use the same sensor geometry, drive voltage and frequency, and feedback capacitor for all studies presented in this Section. The collocation points and the number of harmonics used for the continuum model also are the same for all studies. For easy reference, these values are given in Table 1. There are a number of useful ways to represent the sensed signal. Most directly, it can be given as a complex phasor as presented by V_L in (66). Since the sensed signal is typically small, it is convenient to express it in polar coordinates with the magnitude given in decibels and the phase given in degrees. For an arguably more physically meaningful presentation we can calculate the transconductance and transcapacitance relating the drive electrode voltage and the sense electrode current

$$G_{DS} + \mathrm{i}\omega C_{DS} = \frac{I_s}{V_D} = \frac{-\mathrm{i}\omega C_F V_L}{V_D} \tag{71}$$

One must be cautious with this representation. Because the system has four terminals, it is possible to obtain physically meaningful values of G_{DS} and C_{DS} that are negative even though for passive dielectrics the permittivity and conductivity must be positive. See [16] for a discussion of our experience in this area.

Table 1. Values used by the continuum model in Section 5.

Description	Symbol	Value	Unit
spatial wavelength	λ	1×10^{-3}	m
substrate thickness	d_0	254×10^{-6}	m
nominal electrode height	h	14×10^{-6}	m
nominal meander length	M_L	0.5	m
substrate permittivity	ε_{su}	$2.07\varepsilon_o$	F/m
substrate conductivity	σ_{su}	0	pS/m
sample thickness	d_1	0.1	m
Drive Voltage	V_D	10	V
Drive Frequency	$\omega/2\pi$	1	Hz
Feedback Capacitance	C_F	1317	pF
No. collocation points		40 (20 per surface)	
No. Harmonics, cosine series		500	
No. Harmonics, sine series		500	

In Figure 9 we present the calculated transcapacitance between the driving and sensing electrodes as a function of the electrode height for a sensor in air ($\varepsilon_{sa} = \varepsilon_g = \varepsilon_o$, $\sigma_{sa} = \sigma_g = 0$). It is evident that the effect of the electrode height is important. There is a 10% difference in the capacitance calculated for zero height and for the nominal height of 14 μm. At 40 μm the difference exceeds 20%.

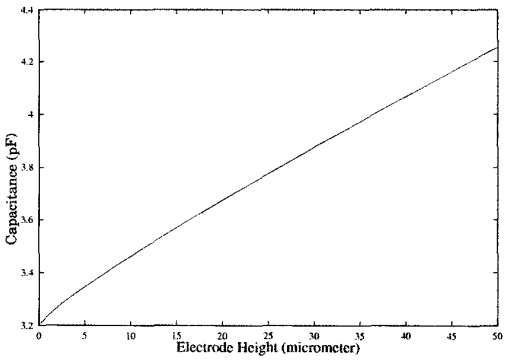

Figure 9. Transcapacitance between the driving and sensing electrodes for a 1 mm wavelength sensor as a function of electrode height.

To demonstrate the multiple solutions of the inverse problem and sensitivity calculations using generalized Eigenanalysis we perform

a study using a material with non-zero conductivity. We calculate the expected response, assuming the electrical properties of a liquid test material (so that it fills the electrode gap region), as $\sigma + i\omega\varepsilon = \varepsilon_o\omega_o(3.614 + i3.015\omega/\omega_o)$ (corresponding to the electric properties of corn oil: 3.015 relative permittivity and 3.614 normalized conductivity where the normalized conductivity is scaled by $\omega_o\varepsilon_o$ and ω_o=1). Next, we use the techniques presented in Section 4 to calculate all possible solutions to the inverse problem.

The values of relative permittivity and normalized conductivity that come from the solution of the inverse problem are shown in Figure 10. There are twenty solutions on the plot. The solution corresponding to the initial forward problem is at coordinates (3.614, 3.015). There is a cluster of artificial solutions around the point $(-3.614, -3.015)$. It should be clear that the only physical solution is the one with positive values of conductivity and permittivity. It is interesting that the artificial solutions are clustered near a point opposite the true solution (scaled by -1). This is possibly due to the symmetry evident in the problem, but should be investigated further.

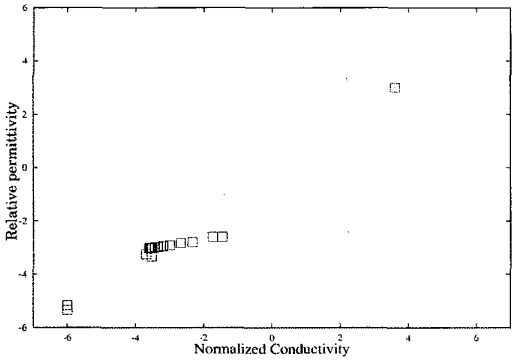

Figure 10. Solutions to the inverse problem; 'normalized conductivity' is conductivity scaled by $\omega_o\varepsilon_o$ where ω_o=1 rad/s.

We also calculate the sensitivity of the estimate to uncertainties in the measurements. The required relations are given by (64), (67), (69), and (70).

Assuming a ±1.0 dB error in the measurement of the response magnitude and a ±1.0 degree error in phase, we find the following limits on the estimated normalized conductivity and relative permittivity: $3.523<\sigma_{sa}<3.705$, $2.970<\varepsilon_{sa}/\varepsilon_o<3.061$, since the material is a liquid and the electrical properties of the gap region are equal to the electrical properties of the sample region.

We have observed that the uncertainty in the estimate depends on the temporal drive frequency. At high frequencies where the permittivity of the test material dominates the response, the estimate of the conductivity is sensitive to small variations in phase. At low frequencies, where the conductivity of the test material dominates the response, the estimate of the permittivity is sensitive to small variations in phase. Figures 11 and 12 show the estimate for the permittivity and conductivity for the material studied above over a wide range of frequencies. Error bars are included that additively account for ± 1.0 dB in measured voltage magnitude and ± 1.0° in phase. Since we are interested in physical solutions, we do not extend the error bars below 1 for the relative permittivity, or below 0 for the normalized conductivity.

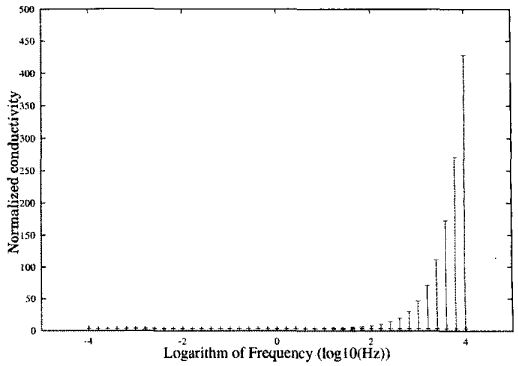

Figure 11. Estimated normalized conductivity including error bars.

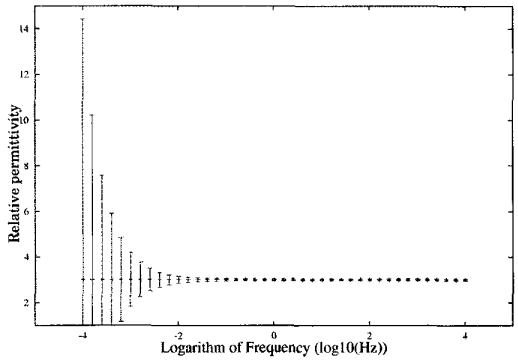

Figure 12. Estimated relative permittivity including error bars.

6 CONCLUSIONS

In this paper we have improved the continuum model by allowing electrode height, calculating the response for the short circuit current measurement mode, and proposed a new non-iterative approach to solving the inverse problem of estimating material properties from a measurement.

For use in our studies with multiple wavelength sensors several practical additions to the model are necessary. In Figures 3 and 4, and throughout this paper, we assume the electrode widths are $\lambda/4$. This is the nominal value, but it may vary within manufacturing tolerances. We determine an average value for the electrode width using a calibration procedure before using the sensor. The changes to the model presented in this paper are straightforward, but perhaps tedious. One rederives the equations while specifying the electrode width as a parameter. We also do not take into account surface effects in this presentation. This is again straightforward; the necessary modification to the continuity equations can be found in [12, 13]. It should be noted that the continuum model does not account for the physically observed 'double layer' capacitance that typically occurs at low frequency. Future work may take this into account.

The use of multiple wavelength sensors for multi-layer samples deserves more discussion. The use of multiple wavelength sensors allows us to probe materials to different penetration depths and enables us to determine material properties of multilayer materials or to estimate discretizations of smooth stratifications of materials. The necessary modifications to the model are included in [12, 13]. and are not derived in detail here. We would like to note that the fusion of data from different wavelength sensors poses an interesting mathematical challenge when solving the inverse problem. The 'multi-parameter' Eigenvalue problem arising from the continuum model will have the following form (similar to (59) in Section 4) for a two layer problem

$$\left[\mathbf{A_1'} - (\sigma_1 + \mathrm{i}\omega\varepsilon_1)\mathbf{B_1} - (\sigma_2 + \mathrm{i}\omega\varepsilon_2)\mathbf{C_1}\right]\mathbf{v_1} = \mathbf{0} \tag{72}$$

$$\left[\mathbf{A_2'} - (\sigma_1 + \mathrm{i}\omega\varepsilon_1)\mathbf{B_2} - (\sigma_2 + \mathrm{i}\omega\varepsilon_2)\mathbf{C_2}\right]\mathbf{v_2} = \mathbf{0} \tag{73}$$

The matrices depend on the width of the layers and the geometry of the sensor. The goal is to find the conductivities and permittivities of the individual layers, σ_1, σ_2, ε_1, and ε_2. There are references that discuss this Eigenvalue problem [17, 18] but a general solver is not available in common software packages. In our laboratory we have developed an iterative method for finding a solution to the two-layer problem but more work needs to be done in this area.

7 APPENDIX

In this Appendix we present the entries for $\mathbf{T}$, $\mathbf{T_1}$, and $\mathbf{T_2}$ used in Sections 2 and 3.

Matrix $\mathbf{T}$ of Section 2 and Matrix $\mathbf{T_1}$ of Section 3 are identical and relate the collocation point voltages of a piecewise continuous representation of a surface voltage profile to coefficients of a truncated Fourier series representation (see Equation (14)). In the following presentation of the entries of $\mathbf{T}$, x_i are the collocation points $1 \le i \le p$ and $x_0 = \lambda/8$ and $x_{p+1} = 3\lambda/8$. Relating the contribution of the driven voltage to the zero harmonic Fourier cosine series coefficient

$$\mathbf{T_{1,1}} = \frac{1}{\lambda}\left(x_1 + \frac{\lambda}{8}\right) \tag{74}$$

The terms relating the driven voltage to the n-th Fourier series coefficient are given by

$$\mathbf{T_{n+1,1}} = \frac{4}{\lambda k_n^2}\left(\frac{\cos(k_n x_0)}{(x_1 - x_0)} - \frac{\cos(k_n x_1)}{(x_1 - x_0)}\right) \tag{75}$$

Relating the contribution of the i-th collocation point voltage to the zero harmonic Fourier cosine series coefficient

$$\mathbf{T_{1,i+1}} = \frac{1}{\lambda}\left(x_{i+1} - x_{i-1}\right) \tag{76}$$

The terms relating the i^{th} collocation point voltage to the n-th Fourier series coefficient are given by

$$\mathbf{T_{n+1,i+1}} = \frac{4}{\lambda k_n^2}\left(\frac{\cos(k_n x_i)}{(x_i - x_{i-1})} + \frac{\cos(k_n x_i)}{(x_{i+1} - x_i)} - \frac{\cos(k_n x_{i-1})}{(x_i - x_{i-1})} - \frac{\cos(k_n x_{i+1})}{(x_{i+1} - x_i)}\right) \tag{77}$$

The terms for the sensing electrode are

$$\mathbf{T_{1,p+2}} = \frac{1}{\lambda}\left(x_1 + \frac{\lambda}{8}\right) \tag{78}$$

$$\mathbf{T_{n+1,p+2}} = \frac{4}{k_n^2}(-1)^n\left(\frac{\cos(k_n x_0)}{(x_1 - x_0)} - \frac{\cos(k_n x_1)}{(x_1 - x_0)}\right) \tag{79}$$

The entries of $\mathbf{T_2}$ relate the collocation point voltages to a sine series representation of part of a piecewise continuous description of the surface voltage profile in the gap region between the electrodes (see (31) and (32)). Matrix $\mathbf{T_2}$ is easily understood and constructed as a product of two matrices

$$\mathbf{T_2} = \mathbf{T_b}\mathbf{T_a}. \tag{80}$$

Matrix $\mathbf{T_a}$ subtracts out the linear portion of the voltage representation along the surface from the driven electrode to sensing electrode. The first column of $\mathbf{T_a}$, related to the driven electrode voltage, is given by

$$\mathbf{T_{a,1,1}} = 0 \tag{81}$$

$$\mathbf{T_{a,i+1,1}} = \frac{\left(x_i - \frac{3\lambda}{8}\right)}{\frac{\lambda}{4}} \tag{82}$$

$$\mathbf{T_{a,p+2,1}} = 0 \tag{83}$$

where $1 \le i \le p$. The last column is given by

$$\mathbf{T_{a,1,p+2}} = 0 \tag{84}$$

$$\mathbf{T_{a,i+1,p+2}} = -\frac{\left(x_i - \frac{\lambda}{8}\right)}{\frac{\lambda}{4}} \tag{85}$$

$$\mathbf{T_{a,p+2,p+2}} = 0 \tag{86}$$

and the diagonal entries are given by

$$\mathbf{T_{a,i+1,i+1}} = 1 \tag{87}$$

All other entries are zero.

Matrix $\mathbf{T_b}$ gives the sine series coefficients. By definition, a Fourier sine series has zero average value; the first row of the matrix is identically zero

$$\mathbf{T_{b,1,i}} = 0 \tag{88}$$

Likewise, the endpoints do not contribute to the series since they are zero by definition; the first and last columns of the matrix are identically zero

$$\mathbf{T_{b,n,1}} = 0 \tag{89}$$

$$\mathbf{T_{b,n,p+2}} = 0 \tag{90}$$

The nonzero entries in $\mathbf{T_b}$ are given by

$$\mathbf{T_{b,n+1,i+1}} = \frac{-8}{\lambda(2k_n)^2}\left[\frac{\sin(2k_n x_i)}{(x_i - x_{i-1})} + \frac{\sin(2k_n x_i)}{(x_{i+1} - x_i)} - \frac{\sin(2k_n x_{i-1})}{(x_i - x_{i-1})} - \frac{\sin(2k_n x_{i+1})}{(x_{i+1} - x_i)}\right] \tag{91}$$

REFERENCES

[1] R. S. Jachowicz and S. D. Senturia, "A thin-film capacitance humidity sensor", Sensors and Actuators, Vol. 2, pp. 171–186, Dec. 1981.

[2] J. S. Kim and D. G. Lee, "Analysis of dielectric sensors for the cure monitoring of resin matrix composite materials", Sensors and Actuators B, Vol. B30, pp. 159–164, Jan. 1996.

[3] K. D. Schierbaum, J. Geiger, U. Weimar, and W. Göpel, "Specific palladium and platinum doping for SnO2-based thin film sensor arrays", Sensors and Actuators B, Vol. 13–14, pp. 143–147, 1993.

[4] H.-E. Endres and S. Drost, "Optimization of the geometry of gas-sensitive interdigital capacitors", Sensors and Actuators B, Vol. 4, pp. 95–98, 1991.

[5] H.-E. Endres, S. Drost, and F. Hunter, "Impedance Spectroscopy on dielectric gas sensors", Sensors and Actuators B, Vol. 22, pp. 7–11, 1994.

[6] R. Zhou, A. Hiermann, K. D. Schierbaum, K. E. Geckeler, and W. Göpel, "Detection of organic solvents with reliable chemical sensors based on cellulose derivatives", Sensors and Actuators B, vol. 24–25, pp. 443–447, 1995.

[7] A. V. Mamishev, *Interdigital Dielectrometry Sensor Design and Parameter Estimation Algorithms for Non-Destructive Materials Evaluation*, PhD Thesis, Department of Electrical Engineering and Computer Science, Massachusetts Institute of Technology, Cambridge, MA, May 1999.

[8] Y. Du, *Measurements and Modeling of Moisture Diffusion Processes in Transformer Insulation using Interdigital Dielectrometry Sensors*, PhD thesis, Department of Electrical Engineering and Computer Science, Massachusetts Institute of Technology, Cambridge, MA, May 1999.

[9] Y. Du, A. V. Mamishev, B. C. Lesieutre, and M. Zahn, "Measurement of Moisture Diffusion as a Function of Temperature in Transformer Pressboard", Proceedings of the IEEE Conference on Electrical Insulation and Dielectric Phenomena, pp. 25–28, Atlanta, GA, Oct. 1998.

[10] A. V. Mamishev, M. Zahn, B. C. Lesieutre, and B. A. Berdnikov, "Influence of geometric parameters on characteristics of an interdigital sensor", Proceedings of the IEEE Conference on Electrical Insulation and Dielectric Phenomena, pp. 550–553, San Francisco, Oct. 1996.

[11] A. V. Mamishev, B. C. Lesieutre, and M. Zahn, "Parameter estimation using an interdigital dielectrometry sensor with finite-element software", Proceedings of the IEEE Conference on Electrical Insulation and Dielectric Phenomena, pp. 234–237, Minneapolis, MN, Oct. 1997.

[12] M. C. Zaretsky, *Parameter Estimation Using Microdielectrometry with Application to Transformer Monitoring*, PhD Thesis, Department of Electrical Engineering and Computer Science, Massachusetts Institute of Technology, Cambridge, MA, May 1987.

[13] M. C. Zaretsky, L. Mouayad, and J. R. Melcher, "Continuum properties from interdigital electrode dielectrometry", IEEE Transactions on Electrical Insulation, Vol. 23, pp. 897–917, Dec. 1988.

[14] Y. Sheiretov, *Dielectrometry Measurements of Moisture Dynamics in Oil-Impregnated Pressboard*, MS Thesis, Department of Electrical Engineering and Computer Science, Massachusetts Institute of Technology, Cambridge, MA, May 1994.

[15] G. H. Golub and C. F. Van Loan, *Matrix Computations*, 3rd ed. The Johns Hopkins University Press, Baltimore, 1996.

[16] A. V. Mamishev, B. C. Lesieutre, and M. Zahn, "Optimization of multi-wavelength interdigital dielectrometry instrumentation and algorithms", IEEE Transactions on Dielectrics and Electrical Insulation, pp. 408–420, 1998.

[17] H. Volkmer, *Multiparameter Eigenvalue Problems and Expansion Theorems*, Lecture Notes in Mathematics Vol. 1356, Springer-Verlag, Berlin, 1988.

[18] F. V. Atkinson, *Multiparameter Eigenvalue Problems, Vol I: Matrices and Compact Operators*, Academic Press, New York, 1972.

This paper is based on a presentation given at the 13th International Conference on Dielectric Liquids, Nara, Japan, 20–25 July 1999.

Manuscript was received on 22 October 1999, in revised form 11 March 2001.